*Journal of Sound and Vibration* (1999) **228**(1), 129–156
*Article No.* jsvi.1999.2406, available online at http://www.idealibrary.com on IDEAL®

# GROUND VIBRATION GENERATED BY A LOAD MOVING ALONG A RAILWAY TRACK

X. SHENG

*Civil Engineering Department, East China Jiaotong University, Nanchang, Jiangxi,* 330013, *People's Republic of China*

AND

C. J. C. JONES, M. PETYT

*I.S.V.R., University of Southampton, Southampton, SO*17 1*BJ, England*

(*Received* 23 *March* 1999, *and in final form* 26 *May* 1999)

The propagation of vibration generated by a harmonic or a constant load moving along a layered beam resting on the layered half-space is investigated theoretically in this paper. The solution to this problem can be used to study the ground vibration generated by the motion of a train axle load on a railway track. In this application, the ground is modelled as a number of parallel viscoelastic layers overlying an elastic half-space or a rigid foundation. The track, including the rails, rail pad, sleepers and ballast, is modelled as an infinite, layered beam structure. The modal nature of propagation in the ground for a chosen set of ground parameters is discussed and the results of the model are presented showing the characteristics of the vibration generated by a constant load and an oscillatory load at speeds below, near to, and above the lowest ground wave speed.



## 1. INTRODUCTION

It is well known that railway operations produce vibrations propagating in the ground which are perceptible in properties at significant distances [1]. Vibrations in the frequency range relevant to the whole-body perception (approximately 4–80 Hz) from tracks onto the ground surface, propagate parallel to the ground surface via Rayleigh wave modes with low rates of attenuation with distance. Observations of high levels of vibration in this frequency range are most commonly associated with heavy axle-load freight operations. However, in recent years, concern has developed over high levels of vibration induced by trains running at high speeds close to or even exceeding the phase velocities of waves propagating in the track structure and the ground [2, 3]. Large increases of vibration level with speed have been predicted [2] and some observations of the effects close to the track have been reported in the literature [3, 4].

0022-460X/99/460129 + 28 $30.00/0 

Analysis of these effects requires realistic models of ground vibration generation and propagation. In particular, it has been shown that it is important to include the effects of both the railway track structure and the layered structure of the ground [5, 6]. Here the term "track structure" is used to encompass the rails, rail supports, the sleepers, the ballast and, when applicable, an embankment.

Jones and Block [7] divided the vibration observed at the track during the passage of a train into two parts. The first consists of the time history of the quasi-static deformation pattern due to successive axles as the train passes a fixed point, and the second is the response to the dynamic loads caused by the acceleration of the masses of the train over the combined irregular profile of the wheels and the track. For the propagation of vibration in the ground, reference [7] used a model of wave propagation from a fixed-point harmonic load on the track. The effect of the movement of the train was introduced as phase terms in the summation of vibration contributions from different sleeper positions along the track. Results of this model were compared with the measurements of vibration from freight trains at a particular site. For these trains, moving at speeds well below the velocities of waves in the track and ground structure, the fixed-point load model satisfactorily represented the propagation of the vibration.

Takemiya and Goda [8] divide the source of vibration excitation from a single axle into three components. The first, similarly to reference [7], is a moving non-harmonic load, the second, a fixed-point dynamic loading at the track, and the third, a moving harmonic load to represent the dynamic vehicle forces. It is proper to model the second of these components as a harmonic load at a fixed point on the track [6] but for trains moving at significant speeds compared to the waves in the track and ground, the first and the third of these components require a model of a moving load.

Reference [6] illustrates the existence of a wave of the combined track and ground propagating along the direction of the track with a speed controlled by, but lower than, the lowest propagating wave in the free, layered ground structure. In soft soil types this wave speed can be lower than the speed of the travel of some passenger trains and it is known by track engineers that the track design must take account of this. In reference [3] large amplitudes of displacement at the track have been measured as the speed of the train is increased towards the critical speed, at the measurement site, of about $50\ \mathrm{m\,s^{-1}}$ (180 km/h).

For the study of the propagation of vibration away from the track for high-speed trains a moving load model is required. The theory of the generation of vibration under the action of moving loads has received considerable attention in the past. Alabi [9, 10] modelled moving loads on a half-space but implemented no model of the track. In reference [11] the ground vibration generated by a moving harmonic rectangular load acting directly on the ground surface with the ground modelled as a half-space is studied. In reference [12] de Barros and Luco present a model with a moving point load on a layered ground. The latter uses the layer transfer matrix approach for the layered ground, first presented by Haskell [13] and Thomson [14], and which is similar to the approach used in the present work. Each of these models is used to study the generation of vibration from trains but does not include the track structure.

Recently, Dieterman and Metrikine [15] used a model of a point harmonic load moving along an elastic layer resting on a rigid foundation to study the existence of critical speeds in the ballast layer. The same authors [16] also produced a model of a constant load moving on a beam on a half-space to study the steady state displacements in the beam at speeds below, near, and exceeding the Rayleigh wave speed.

Krylov [2] studied ground vibration from the whole set of moving loads of a train on a track structure, but taking only a single Rayleigh wave type into account in the ground part of the model. In reference [4] Krylov includes some of the effects of a layered ground into the same modelling approach by using a frequency-dependent Rayleigh wave speed.

Along with their presentation of measurements in reference [3] Madshus and Kaynia report the development of a model which includes a moving load on a railway/embankment structure modelled using finite elements which is then coupled at a series of points, to a layered ground model via Green's functions which are calculated using the dynamic stiffness matrix theory developed by Kausel and Roësset [17].

In this paper the model of reference [6] is extended to encompass the effects of a load moving on a track on the layered ground. The model deals with both loads that are constant and also those that have a non-zero frequency in the moving frame of reference. The ground is modelled as a structure of the three-dimensional viscoelastic layers overlying either a half-space or a rigid foundation. The track is modelled by a single rail beam, rail pad and a sleeper mass layer supported by a viscoelastic ballast layer. In section 2, the differential equations of motion of the railway and the Navier's equations for the ground are presented. Section 3, outlines the calculation of the ground dynamic flexibility matrix making use of the theory presented by the authors in reference [6]. In section 4, the railway and the ground are coupled, rendering it possible to calculate the Fourier-transformed response of the ground surface. These are used for calculating the displacements and velocities as a function of Cartesian co-ordinates either through a two-dimensional inverse FFT, or a Fourier transform implemented through a specialized quadrature. Although the load is applied with a single non-zero frequency or at zero frequency, the ground vibration is a transient with a broad band of frequency content because of the movement of the load. The spectra of the transient ground vibrations are important in practice and are therefore investigated in section 5. Section 6 presents a number of results of the model to investigate the effects of the moving load on the generation of vibration.

## 2. THE DIFFERENTIAL EQUATIONS OF MOTION OF THE RAILWAY–GROUND SYSTEM

A diagram of the model is presented in Figure 1. The railway is infinite in length and is aligned in the $x$ direction. It has a contact width $2b$ with the ground. The rails are modelled as a single Euler beam with mass per unit length of track $m_R$ and bending stiffness $EI$. The sleepers are modelled as a distributed mass $m_S$ per unit

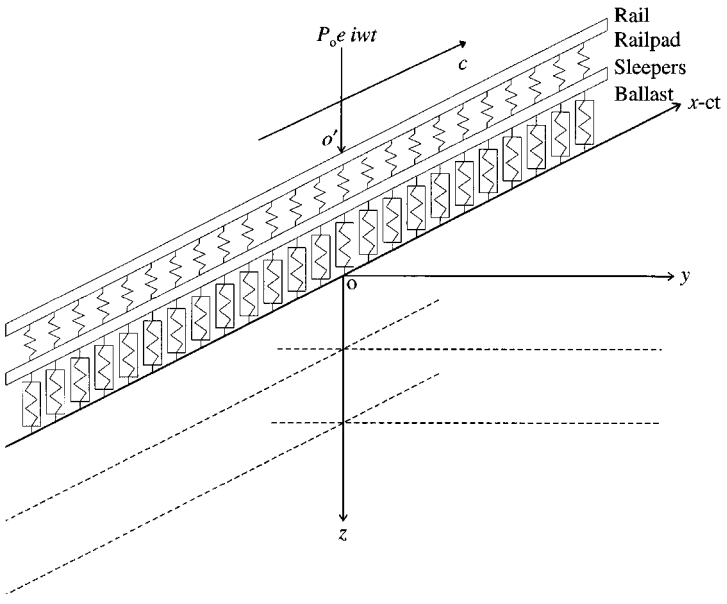


Figure 1. Diagram of the model of track on layered ground.

length of track. The rail pads are represented as a distributed vertical spring stiffness $k_P$ between the rail beam and the sleeper mass. The ballast is modelled as a viscoelastic layer with a width $2b$ and a mass per unit length $m_B$. For the ballast layer, only the vertical stiffness $K_B$ is taken into account. All track components are attributed damping properties by the use of complex stiffness parameters, i.e., each of the stiffness parameters defined above are complex being derived from a real stiffness value and an associated loss factor, for example, $\eta_p \operatorname{sgn}(\omega)$ for the rail pads where $\operatorname{sgn}(\omega)$ means the sign of the frequency $\omega$.

The moving load is assumed harmonic with an angular frequency $\Omega$, and an amplitude $P_0$. When $\Omega$ is set to zero, the load becomes a moving constant load. At time $t$, the distance from the load to the point $O$' (see Figure 1) is $ct$, where $c$ is the speed of the moving load. The vertical displacements of the rail beam and the sleeper mass are denoted by $w_1(x, t)$, $w_2(x, t)$, respectively, and the vertical displacement at the centreline in the contact plane (i.e., the $x$-axis) by $w_3(x, t)$. Furthermore, it is supposed that the contact force in the contact plane is normal and is evenly distributed in the $y$ direction from $y = -b$ to $y = b$, the per-length value of which in the $x$ direction is $F_3(x, t)$.

The plane $Oxy$ represents the ground surface, below which the ground consists of a number, $n$, layers. The $n$th layer overlies a half-space or a rigid foundation, which is termed the layer number $n + 1$. The material constants of layer $j$ are the Young's modulus, $E_j$, Possion ratio, $v_j$, density, $\rho_j$, loss factor, $\eta_j \operatorname{sgn}(\omega)$, and thickness, $h_j$. If layer $n + 1$ is a half-space, its material constants are $E_{n+1}$, $v_{n+1}$,$\rho_{n+1}$ and $\eta_{n+1} \operatorname{sgn}(\omega)$.

The differential equations of motion of the railway are as follows.

For the rail beam,

$$EI\frac{\partial^4 w_i(x,t)}{\partial x^4} + m_R\frac{\partial^2 w_1(x,t)}{\partial t^2} + k_P[w_1(x,t) - w_2(x,t)] = \delta(x - ct)P_0\,\mathrm{e}^{\mathrm{i}\Omega t} \quad (1)$$

where $\delta(.)$ is the Dirac-delta function.

For the sleeper mass,

$$m_S\frac{\partial^2 w_2(x,t)}{\partial t^2} + k_P[w_2(x,t) - w_1(x,t)] = -F_2(x,t) \quad (2)$$

and for the ballast layer a linear spring stiffness with a consistent mass approximation is used so that

$$\frac{m_B}{6}\begin{bmatrix}2 & 1\\ 1 & 2\end{bmatrix}\begin{Bmatrix}\dfrac{\partial^2 w_2(x,t)}{\partial t^2}\\ \dfrac{\partial^2 w_3(x,t)}{\partial t^2}\end{Bmatrix} + k_B\begin{bmatrix}1 & -1\\ -1 & 1\end{bmatrix}\begin{Bmatrix}w_2(x,t)\\ w_3(x,t)\end{Bmatrix} = \begin{Bmatrix}F_2(x,t)\\ -F_3(x,t)\end{Bmatrix}, \quad (3)$$

where $F_2(x,t)$ is the force per unit length of track between the sleeper mass and the ballast.

The differential equations of motion of the ground are Navier's equations. For the $j$th layer, they are

$$\begin{aligned}(\lambda_j + \mu_j)\frac{\partial \Delta_j}{\partial x} + \mu_j\nabla^2 u_j &= \rho_j\frac{\partial^2 u_j}{\partial t^2}\\ (\lambda_j + \mu_j)\frac{\partial \Delta_j}{\partial y} + \mu_j\nabla^2 v_j &= \rho_j\frac{\partial^2 v_j}{\partial t^2} \qquad (j = 1, 2, \ldots, n+1),\\ (\lambda_j + \mu_j)\frac{\partial \Delta_j}{\partial z} + \mu_j\nabla^2 w_j &= \rho_j\frac{\partial^2 w_j}{\partial t^2}\end{aligned} \quad (4)$$

where, $\lambda_j$ and $\mu_j$ are the Lamé constants of the $j$th layer, determined from the Young's modulus and the Poisson ratio by

$$\lambda_j = \frac{v_j E_j(1 + \mathrm{i}\eta_j\,\mathrm{sgn}(\omega))}{(1+v_j)(1-2v_j)}, \quad \mu_j = \frac{v_j E_j(1 + \mathrm{i}\eta_j\,\mathrm{sgn}(\omega))}{2(1+v_j)} \quad (5)$$

The displacements in the $x$, $y$, $z$ directions of a point $(x, y, z)$ in the layer (where $z \in [0, h_j]$), are $u_j = u_j(x, y, z, t)$, $v_j = v_j(x, y, z, t)$ and $w_j = w_j(x, y, z, t)$,

$$\Delta_j = \frac{\partial u_j}{\partial x} + \frac{\partial v_j}{\partial y} + \frac{\partial w_j}{\partial z} \quad (6)$$

and $\nabla^2$ is the Laplace operator.

Now applying the single spatial Fourier transform pairs

$$\bar{f}(\beta) = \int_{-\infty}^{\infty} f(x)\,\mathrm{e}^{-\mathrm{i}\beta x}\,\mathrm{d}x, \qquad f(x) = \frac{1}{2\pi}\int_{-\infty}^{\infty} \bar{f}(\beta)\,\mathrm{e}^{\mathrm{i}\beta x}\,d\beta \tag{7}$$

to equations (1)–(3), and double spatial Fourier transform pairs

$$\bar{f}(\beta,\gamma) = \int_{-\infty}^{\infty}\int_{-\infty}^{\infty} f(x,y)\,\mathrm{e}^{-i(\beta x+\gamma y)}\,\mathrm{d}x\mathrm{d}y,$$

$$f(x,y) = \frac{1}{4\pi^2}\int_{-\infty}^{\infty}\int_{-\infty}^{\infty} \bar{f}(\beta,\gamma)\,\mathrm{e}^{i(\beta x+\gamma y)}\,d\beta\,d\gamma, \tag{8}$$

to equations (4), yields

$$EI\beta^4\bar{w}_1(\beta,t) + m_R\frac{\partial^2\bar{w}_1(\beta,t)}{\partial t^2} + k_P[\bar{w}_1(\beta,t) - \bar{w}_2(\beta,t)] = \mathrm{e}^{\mathrm{i}(\Omega-\beta c)t}P_0, \tag{9}$$

$$m_S\frac{\partial^2\bar{w}_2(\beta,t)}{\partial t^2} + k_P[\bar{w}_2(\beta,t) - \bar{w}_1(\beta,t)] = -\bar{F}_2(\beta,t), \tag{10}$$

$$\frac{m_B}{6}\begin{bmatrix}2 & 1\\ 1 & 2\end{bmatrix}\begin{Bmatrix}\dfrac{\partial^2\bar{w}_2(\beta,t)}{\partial t^2}\\[2ex] \dfrac{\partial^2\bar{w}_3(\beta,t)}{\partial t^2}\end{Bmatrix} + k_B\begin{bmatrix}1 & -1\\ -1 & 1\end{bmatrix}\begin{Bmatrix}\bar{w}_2(\beta,t)\\ \bar{w}_3(\beta,t)\end{Bmatrix} = \begin{Bmatrix}\bar{F}_2(\beta,t)\\ -\bar{F}_3(\beta,t)\end{Bmatrix}, \tag{11}$$

$$(\lambda_j+\mu_j)\,\mathrm{i}\beta\bar{\Delta}_j + \mu_j\left(\frac{d^2\bar{u}_j}{dz^2} - \beta^2\bar{u}_j - \gamma^2\bar{u}_j\right) = \rho_j\frac{\partial^2\bar{u}_j}{dt^2},$$

$$(\lambda_j+\mu_j)\,\mathrm{i}\gamma\bar{\Delta}_j + \mu_j\left(\frac{d^2\bar{v}_j}{dz^2} - \beta^2\bar{v}_j - \gamma^2\bar{v}_j\right) = \rho_j\frac{\partial^2\bar{v}_j}{dt^2},$$

$$(\lambda_j+\mu_j)\frac{\partial\bar{\Delta}_j}{\partial z} + \mu_j\left(\frac{d^2\bar{w}_j}{dz^2} - \beta^2\bar{w}_j - \gamma^2\bar{w}_j\right) = \rho_j\frac{\partial^2\bar{w}_j}{dt^2}, \tag{12}$$

where the bar notation is used to represent the quantities transformed into the wave number domain, e.g.,

$$\bar{w}_1(\beta,t) = \int_{-\infty}^{\infty} w_1(x,t)\,\mathrm{e}^{-\mathrm{i}\beta x}\,\mathrm{d}x, \qquad \bar{u}_j = \bar{u}_j(\beta,\gamma,z,t)$$

$$= \int_{-\infty}^{\infty}\int_{-\infty}^{\infty} u_j(x,y,z,t)\,\mathrm{e}^{-\mathrm{i}(\beta x+\gamma y)}\,\mathrm{d}x\mathrm{d}y.$$

Equations (9)–(12) are the Fourier transformed differential equations of motion of the railway–ground system. By taking into account the right-hand term in equation (9) and including the damping by using the complex moduli and stiffness

parameters, steady state solutions of equations (9)–(12) may be found, i.e.,

$$\begin{aligned}
\bar{w}_1(\beta, t) &= \tilde{w}_1(\beta)\,\mathrm{e}^{\mathrm{i}(\Omega-\beta c)t},\\
\bar{w}_2(\beta, t) &= \tilde{w}_2(\beta)\,\mathrm{e}^{\mathrm{i}(\Omega-\beta c)t},\\
\bar{w}_3(\beta, t) &= \tilde{w}_3(\beta)\,\mathrm{e}^{\mathrm{i}(\Omega-\beta c)t},\\
\bar{F}_2(\beta, t) &= \tilde{F}_2(\beta)\,\mathrm{e}^{\mathrm{i}(\Omega-\beta c)t},\\
\bar{F}_3(\beta, t) &= \tilde{F}_3(\beta)\,\mathrm{e}^{\mathrm{i}(\Omega-\beta c)t},\\
\bar{u}_j(\beta, \gamma, z, t) &= \tilde{u}_j(\beta, \gamma, z)\,\mathrm{e}^{\mathrm{i}(\Omega-\beta c)t},\\
\bar{v}_j(\beta, \gamma, z, t) &= \tilde{v}_j(\beta, \gamma, z)\,\mathrm{e}^{\mathrm{i}(\Omega-\beta c)t},\\
\bar{w}_j(\beta, \gamma, z, t) &= \tilde{w}_j(\beta, \gamma, z)\,\mathrm{e}^{\mathrm{i}(\Omega-\beta c)t},\\
\bar{\Delta}_j(\beta, \gamma, z, t) &= \tilde{\Delta}_j(\beta, \gamma, z)\,\mathrm{e}^{i(\Omega-\beta c)t}.
\end{aligned} \tag{13}$$

If the inverse Fourier transform of $\tilde{u}_j(\beta, \gamma, z)$ is denoted by $u_j^*(x, y, z)$, from equation (13) the inverse Fourier transform of $\bar{u}_j(\beta, \gamma, z, t)$ is given by

$$u_j(x, y, z, t) = u_j^*(x - ct, y, z)\,e^{i\Omega t} \tag{14}$$

Equation (14) shows that the time-varying displacement field $u_j(x, y, z, t)$ is just the propagation of the wave field $u_j^*(x, y, z)\,e^{i\Omega t}$ in the $x$ direction at the load speed $c$. For fixed values of $y$ and $z$, if $u_j^*(x, y, z)$ is known for a number of successive values of $x$ within $x_0 - \varepsilon \leqslant x \leqslant x_0 + \varepsilon$, where $\varepsilon$ is a positive number, the time history of the displacement of point $(x_0, y, z)$ is determined by equation (14). For the calculation of a large number of values $u_j^*(x, y, z)$ to form a time history of which the spectrum may be calculated, it is appropriate to use an FFT algorithm rather than implementing a Fourier transform using a specialized quadrature. The latter method is efficient for the calculation at a single point $(x, y, z)$ [6].

Substituting equation (13) into equations (9)–(12), and putting

$$\omega = \Omega - \beta c \tag{16}$$

gives

$$EI\beta^4\tilde{w}_1(\beta) - \omega^2 m_R\tilde{w}_1(\beta) + k_P[\tilde{w}_1(\beta) - \tilde{w}_2(\beta)] = P_0, \tag{17}$$

$$-\omega^2 m_S\tilde{w}_2(\beta) + k_P[\tilde{w}_2(\beta) - \tilde{w}_1(\beta)] = -\tilde{F}_2(\beta), \tag{18}$$

$$-\frac{m_B\omega^2}{6}\begin{bmatrix}2 & 1\\ 1 & 2\end{bmatrix}\begin{Bmatrix}\tilde{w}_2(\beta)\\ \tilde{w}_3(\beta)\end{Bmatrix} + k_B\begin{bmatrix}1 & -1\\ -1 & 1\end{bmatrix}\begin{Bmatrix}\tilde{w}_2(\beta)\\ \tilde{w}_3(\beta)\end{Bmatrix} = \begin{Bmatrix}\tilde{F}_2(\beta)\\ -\tilde{F}_3(\beta)\end{Bmatrix}, \tag{19}$$

$$\begin{aligned}
&(\lambda_j + \mu_j)\mathrm{i}\beta\tilde{\Delta}_j + \mu_j\left[\frac{\mathrm{d}^2\tilde{u}_j}{\mathrm{d}z^2} - \left(\beta^2 + \gamma^2 - \frac{\omega^2\rho_j}{\mu_j}\right)\tilde{u}_j\right] = 0\\
&(\lambda_j + \mu_j)\mathrm{i}\gamma\tilde{\Delta}_j + \mu_j\left[\frac{\mathrm{d}^2\tilde{v}_j}{\mathrm{d}z^2} - \left(\beta^2 + \gamma^2 - \frac{\omega^2\rho_j}{\mu_j}\right)\tilde{v}_j\right] = 0 \quad (j = 1, 2, \ldots, n+1).\\
&(\lambda_j + \mu_j)\frac{\partial\bar{\Delta}_j}{\partial z} + \mu_j\left[\frac{\mathrm{d}^2\tilde{w}_j}{\mathrm{d}z^2} - \left(\beta^2 + \gamma^2 - \frac{\omega^2\rho_j}{\mu_j}\right)\tilde{w}_j\right] = 0
\end{aligned} \tag{20}$$

Comparing equations (17)–(20) with reference [6], it can be concluded that the solution of equations (17)–(20) is the same as determining the Fourier transformed responses when a harmonic load with amplitude $P_0$ and angular frequency $\omega$ (determined by equation (16)) acts at the head of the rail just above the origin point. Therefore, the approach developed in reference [6], which will be briefly summarized in sections 3 and 4 for the analysis of the layered ground and the coupling of the track structure to the ground model, can be applied here.

## 3. ANALYSIS FOR THE LAYERED GROUND IN THE WAVE NUMBER DOMAIN

### 3.1. FOR A GROUND LAYER

For the $j$th layer of the ground, the stresses are denoted by $\tau_{xzj}(x, y, z, t)$, $\tau_{yzj}(x, y, z, t)$, $\tau_{zzj}(x, y, z, t)$, where $z \varepsilon [0, h_j]$. The Fourier transforms of these are $\bar{\tau}_{xzj}(\beta, \gamma, z, t)$, $\bar{\tau}_{yzj}(\beta, \gamma, z, t)$, $\bar{\tau}_{zzj}(\beta, \gamma, z, t)$. As in equation (13), the transformed stresses, $\bar{\tau}_{xzj}(\beta, \gamma, z, t)$, etc., can be written as

$$\begin{aligned}
\bar{\tau}_{xzj}(\beta, \gamma, z, t) &= \tilde{\tau}_{xzj}(\beta, \gamma, z)\, \mathrm{e}^{\mathrm{i}(\Omega - \beta c)t} \\
\bar{\tau}_{yzj}(\beta, \gamma, \mathrm{z}, t) &= \tilde{\tau}_{yzj}(\beta, \gamma, z)\, \mathrm{e}^{\mathrm{i}(\Omega - \beta c)t} \qquad (j = 1, 2, \ldots, n+1), \\
\bar{\tau}_{zzj}(\beta, \gamma, \mathrm{z}, t) &= \tilde{\tau}_{zzj}(\beta, \gamma, z)\, \mathrm{e}^{\mathrm{i}(\Omega - \beta c)t}
\end{aligned} \tag{21}$$

so that $\tilde{\tau}_{xzj}(\beta, \gamma, z)$, etc., represent transformed steady state solutions for the moving frame of reference of the load.

Putting

$$\begin{aligned}
\{\tilde{\mathbf{u}}\}_{j0} &= (\tilde{u}_j(\beta, \gamma, 0), \tilde{v}_j(\beta, \gamma, 0), \tilde{w}_j(\beta, \gamma, 0))^{\mathrm{T}}, \\
\{\tilde{\boldsymbol{\tau}}\}_{j0} &= (\tilde{\tau}_{xzj}(\beta, \gamma, 0), \tilde{\tau}_{yzj}(\beta, \gamma, 0), \tilde{\tau}_{zzj}(\beta, \gamma, 0))^{\mathrm{T}}, \\
\{\tilde{\mathbf{S}}\}_{j0} &= \begin{Bmatrix} \{\tilde{u}\}_{j0} \\ \{\tilde{\tau}\}_{j0} \end{Bmatrix}
\end{aligned} \tag{22}$$

and

$$\begin{aligned}
\{\tilde{\mathbf{u}}\}_{j1} &= (\tilde{u}_j(\beta, \gamma, h_j), \tilde{v}_j(\beta, \gamma, h_j), \tilde{w}_j(\beta, \gamma, h_j))^{\mathrm{T}}, \\
\{\tilde{\boldsymbol{\tau}}\}_{j1} &= (\tilde{\tau}_{xzj}(\beta, \gamma, h_j), \tilde{\tau}_{yzj}(\beta, \gamma, h_j), \tilde{\tau}_{zzj}(\beta, \gamma, h_i))^{\mathrm{T}}, \\
\{\tilde{\mathbf{S}}\}_{j0} &= \begin{Bmatrix} \{\tilde{u}\}_{j0} \\ \{\tilde{\tau}\}_{j0} \end{Bmatrix},
\end{aligned} \tag{23}$$

where $\{\tilde{\mathbf{S}}\}_{j0}$ is for the top of $j$th layer, and $\{\tilde{\mathbf{S}}\}_{j1}$ is for its bottom, it can be shown that [6]

$$\{\tilde{\mathbf{S}}\}_{j1} = \mathrm{e}^{\alpha_{j1} h_j} [\mathbf{A}]_{j1} [\mathbf{A}]_{j0}^{-1} \{\tilde{\mathbf{S}}\}_{j0} \quad (j = 1,2, \ldots, n) \tag{24}$$

where $[\mathbf{A}]_{j1}$, $[\mathbf{A}]_{j0}$ are $6 \times 6$ matrices. The elements of these matrices and $\alpha_{j1}$ are determined by the parameters of the layer and $\omega$. The expressions for these matrices are presented in reference [6].

### 3.2. FOR A HALF-SPACE

Putting

$$\begin{aligned} \{\tilde{\mathbf{u}}\}_{n+1,0} &= (\tilde{u}_{n+1}(\beta, \gamma, 0), \tilde{v}_{n+1}(\beta, \gamma, 0), \tilde{w}_{n+1}(\beta, \gamma, 0))^{\mathrm{T}}, \\ \{\tilde{\boldsymbol{\tau}}\}_{n+1,0} &= (\tilde{\tau}_{xz,n+1}(\beta, \gamma, 0), \tilde{\tau}_{yz,n+1}(\beta, \gamma, 0), \tilde{\tau}_{zz,n+1}(\beta, \gamma, 0))^{\mathrm{T}}, \end{aligned} \tag{25}$$

similar to equation (24), one can show that [6]

$$\{\tilde{\mathbf{u}}\}_{n+1,0} = [\mathbf{R}][\mathbf{S}]^{-1}\{\tilde{\boldsymbol{\tau}}\}_{n+1,0} \tag{26}$$

where $[\mathbf{R}]$ and $[\mathbf{S}]$ are $3 \times 3$ matrices the elements of which are determined by the parameters of the half-space and $\omega$. Again the expressions for $[\mathbf{R}]$ and $[\mathbf{S}]$ may be found in reference [6].

### 3.3. FOR THE WHOLE LAYERED GROUND

The "transfer" matrices relating the stresses and displacements at the top and bottom of a layer or at the surface of a half-space may be used to model a complete multi-layered half-space by the method first shown by Haskell [13] and Thomson [14]. Noticing that

$$\{\tilde{\mathbf{S}}\}_{11} = \{\tilde{\mathbf{S}}\}_{20},\ \{\tilde{\mathbf{S}}\}_{21} = \{\tilde{\mathbf{S}}\}_{30}, \ldots, \{\tilde{\mathbf{S}}\}_{n-1,1} = \{\tilde{S}\}_{n0},$$

it can be shown from equation (24) that

$$\{\tilde{\mathbf{S}}\}_{n1} = \mathrm{e}^{\Sigma_{i=1}^{n} \alpha_{j1} h_j} [\mathbf{A}]_{n1}[\mathbf{A}]_{n0}^{-1}[\mathbf{A}]_{n-1,1}[\mathbf{A}]_{n-1,0}^{-1} \cdots [\mathbf{A}]_{11}[\mathbf{A}]_{10}^{-1}\{\tilde{\mathbf{S}}\}_{10}. \tag{27}$$

Putting

$$[\mathbf{T}] = [\mathbf{A}]_{n1}[\mathbf{A}]_{n0}^{-1}[\mathbf{A}]_{n-1,1}[\mathbf{A}]_{n-1,0}^{-1} \cdots [\mathbf{A}]_{11}[\mathbf{A}]_{10}^{-1} = \begin{bmatrix} [\mathbf{T}]_{11} & [\mathbf{T}]_{12} \\ [\mathbf{T}]_{21} & [\mathbf{T}]_{22} \end{bmatrix}, \tag{28}$$

where $[\mathbf{T}]_{11}$ etc., are $3 \times 3$ matrices, equation (27) becomes

$$\begin{Bmatrix} \{\tilde{\mathbf{u}}\}_{n1} \\ \{\tilde{\boldsymbol{\tau}}\}_{n1} \end{Bmatrix} = \mathrm{e}^{\Sigma_{i=1}^{n} \alpha_{j1} h_j} \begin{bmatrix} [\mathbf{T}]_{11} & [\mathbf{T}]_{12} \\ [\mathbf{T}]_{21} & [\mathbf{T}]_{22} \end{bmatrix} \begin{Bmatrix} \{\tilde{\mathbf{u}}\}_{10} \\ \{\tilde{\boldsymbol{\tau}}\}_{10} \end{Bmatrix}, \tag{29}$$

Three cases may be encountered:

(1) If the $(n+1)$th layer is a half-space, then $\{\tilde{\mathbf{u}}\}_{n+1,0} = \{\tilde{\mathbf{u}}\}_{n1}$, $\{\tilde{\boldsymbol{\tau}}\}_{n+1,0} = \{\tilde{\boldsymbol{\tau}}\}_{n1}$. From equations (26) and (29), this yields

$$\{\tilde{\mathbf{u}}\}_{10} = [\mathbf{Q}]\{\tilde{\boldsymbol{\tau}}\}_{10}, \tag{30}$$

where $[\mathbf{Q}]$ is a $3 \times 3$ matrix, and

$$[\mathbf{Q}] = \begin{bmatrix} Q_{11} & Q_{12} & Q_{13} \\ Q_{21} & Q_{22} & Q_{23} \\ Q_{31} & Q_{32} & Q_{33} \end{bmatrix} = ([\mathbf{R}][\mathbf{S}]^{-1}[\mathbf{T}]_{21} - [\mathbf{T}]_{11})^{-1}([\mathbf{T}]_{12} - [\mathbf{R}][\mathbf{S}]^{-1}[\mathbf{T}]_{22}). \tag{31}$$

(2) If the $(n+1)$th layer is a rigid foundation, so that $\{\tilde{\mathbf{u}}\}_{n+1,0} = \{\tilde{\mathbf{u}}\}_{n1} = 0$, from equation (29), equation (30) can also be obtained with

$$[\mathbf{Q}] = -[\mathbf{T}]_{11}^{-1}[\mathbf{T}]_{12}. \tag{32}$$

(3) If the ground is comprised of only a half-space (now $n = 0$), equation (26) gives equation (30) with

$$[\mathbf{Q}] = [\mathbf{R}][\mathbf{S}]^{-1}. \tag{33}$$

Equation (30) shows the relation between the Fourier transformed displacement vector and the Fourier transformed stress vector on the ground surface. This relation makes use of the Fourier transformed dynamic flexibility matrix of the ground (if the load is not moving, as defined in reference [6], matrix $[\mathbf{Q}]$ gives the Fourier transformed dynamic flexibility matrix of the ground).

The formulae developed in reference [6] for $[\mathbf{A}]_{j1}$, $[\mathbf{A}]_{j0}$, $[\mathbf{R}]$, $[\mathbf{S}]$, are valid only when $\omega \neq 0$. From equation (16) one can see that $\omega$ is dependent on $\beta$, and $\omega = 0$ when $\beta = \Omega/c$. In this case, the formulae for $[\mathbf{A}]_{j1}$, $[\mathbf{A}]_{j0}$, $[\mathbf{S}]$, $[\mathbf{R}]$ that are presented in reference [6] must be modified to make them computable [18].

It is worth noting some properties of $Q_{13}$, $Q_{23}$ and $Q_{33}$ namely that:

(1) $Q_{13}(\beta, \gamma)$ is an even function of $\gamma$; and $Q_{13}(0, \gamma) = 0$ for any $\gamma$;
(2) $Q_{23}(\beta, \gamma)$ is an odd function of $\gamma$;
(3) $Q_{33}(\beta, \gamma)$ is an even function of $\gamma$.

These and other properties of the matrix $[\mathbf{Q}]$ that lead to the efficient calculation are discussed in greater detail in reference [18].

## 4. COUPLING OF THE GROUND WITH THE RAILWAY AND THE DISPLACEMENTS AND VELOCITIES OF THE GROUND SURFACE

Coupling of the ground with the railway track can be carried out by taking into account the continuity of the displacements and the equilibrium of the stresses in

the plane of contact between them, i.e.,

$$w_1(x, 0, 0, t) = w_3(x, t), \tag{34}$$

$$\tau_{zz1}(x, y, 0, t) = \begin{cases} -\dfrac{F_3(x, t)}{2b}, & |y| \leqslant b, \\ 0 & \text{elsewhere}, \end{cases} \tag{35}$$

where

$$w_1(x, 0, 0, t) = \frac{1}{4\pi^2} \int_{-\infty}^{\infty} \int_{-\infty}^{\infty} \bar{w}_1(\beta, \gamma, 0, t)\, \mathrm{e}^{\mathrm{i}(\beta x + \gamma y)}\, \mathrm{d}\beta\, \mathrm{d}\gamma\,|_{y=0}$$

$$= \frac{1}{4\pi^2} \int_{-\infty}^{\infty} \int_{-\infty}^{\infty} \bar{w}_1(\beta, \gamma, 0, t)\, \mathrm{e}^{\mathrm{i}\beta x}\, \mathrm{d}\beta\, \mathrm{d}\gamma. \tag{36}$$

Now Fourier transforming equation (34) with respect to $x$ and taking into account equation (36), yields

$$\bar{w}_3(\beta, t) = \frac{1}{2\pi} \int_{-\infty}^{\infty} \bar{w}_1(\beta, \gamma, 0, t)\, \mathrm{d}\gamma. \tag{37}$$

The double Fourier transform of equation (35), gives

$$\bar{\tau}_{zz1}(\beta, \gamma, 0, t) = -\bar{F}_3(\beta, t) \frac{\sin \gamma b}{\gamma b}. \tag{38}$$

Using the reduction to steady state solutions in the moving frame of reference that has already been expressed in equations (13) and (21), equations (37) and (38) can be restated as

$$\tilde{w}_3(\beta) = \frac{1}{2\pi} \int_{-\infty}^{\infty} \tilde{w}_1(\beta, \gamma, 0)\, \mathrm{d}\gamma \tag{39}$$

$$\tilde{\tau}_{zz1}(\beta, \gamma, 0) = -\tilde{F}_3(\beta) \frac{\sin \gamma b}{\gamma b}. \tag{40}$$

The simplifying assumption that only the vertical component of stress between the track and the ground need be used, is now invoked. (Only the vertical mechanics of the track structure are included in the model.) Thus, the stress field $\{\tilde{\boldsymbol{\tau}}\}_{10}$ is described only by $\tilde{\tau}_{zz1}(\beta, \gamma, 0)$ and equation (30) gives the transformed vertical displacement at the track/ground interface as

$$\tilde{w}_1(\beta, \gamma, 0) = -Q_{33} \tilde{F}_3(\beta) \frac{\sin \gamma b}{\gamma b}$$

and from equation (39) one gets

$$\tilde{w}_3(\beta) = \left( -\frac{1}{2\pi} \int_{-\infty}^{\infty} Q_{33} \frac{\sin \gamma b}{\gamma b}\, \mathrm{d}\gamma \right) \tilde{F}_3(\beta). \tag{41}$$

The bracketed term on the right-hand side of equation (41) represents the flexibility of the ground that is subject to the force applied by the track. Denoting this as $\tilde{H}(\beta)$ and using the fact that the integrand is an even function of $\gamma$, gives

$$\tilde{H}(\beta) = -\frac{1}{\pi}\int_0^\infty Q_{33}\frac{\sin\gamma b}{\gamma b}\,\mathrm{d}\gamma. \tag{42}$$

which is calculable from the ground model presented in section 3. Now equation (39) is restated as

$$\tilde{w}_3(\beta) = \tilde{H}(\beta)\tilde{F}_3(\beta). \tag{43}$$

Substitution of equation (43) into equations (17)–(19) allows them to be solved to eliminate $\tilde{w}_1(\beta)$, $\tilde{w}_2(\beta)$, $\tilde{F}_2(\beta)$, $\tilde{w}_3(\beta)$ and to calculate $\tilde{F}_3(\beta)$. Then $\tilde{\tau}_{zz1}(\beta, \gamma, 0)$ is known via equation (40) and equation (30) shows

$$\begin{aligned}
\tilde{u}_1(\beta, \gamma, 0) &= -Q_{13}\frac{\sin\gamma b}{\gamma b}\tilde{F}_3(\beta),\\
\tilde{v}_1(\beta, \gamma, 0) &= -Q_{23}\frac{\sin\gamma b}{\gamma b}\tilde{F}_3(\beta),\\
\tilde{w}_1(\beta, \gamma, 0) &= -Q_{33}\frac{\sin\gamma b}{\gamma b}\tilde{F}_3(\beta).
\end{aligned} \tag{44}$$

From equation (13) the time-varying Fourier transformed displacements of the ground surface can be obtained.

If the inverse Fourier transforms of $\tilde{u}_1(\beta, \gamma, 0)$, $\tilde{v}_1(\beta, \gamma, 0)$, $\tilde{w}_1(\beta, \gamma, 0)$ are denoted by $u_{10}^*(x, y)$, $v_{10}^*(x, y)$, $w_{10}^*(x, y)$, respectively, i.e.,

$$u_{10}^*(x, y) = \frac{1}{4\pi^2}\int_{-\infty}^{\infty}\int_{-\infty}^{\infty}\tilde{u}_1(\beta, \gamma, 0)\,\mathrm{e}^{\mathrm{i}(\beta x + \gamma y)}\,\mathrm{d}\gamma\,\mathrm{d}\gamma, \tag{45}$$

the displacements of the ground surface, denoted by $u_{10}(x, y, t)$, $v_{10}(x, y, t)$, $w_{10}(x, y, t)$, are as follows:

$$\begin{aligned}
u_{10}(x, y, t) &= u_{10}^*(x - ct, y)\,e^{i\Omega t},\\
v_{10}(x, y, t) &= v_{10}^*(x - ct, y)\,e^{i\Omega t},\\
\mathrm{w}_{10}(x, y, t) &= w_{10}^*(x - ct, y)\,e^{\mathrm{i}\Omega t},
\end{aligned} \tag{46}$$

and specifically at $t = 0$,

$$\begin{aligned}
u_{10}(x, y, 0) &= u_{10}^*(x, y),\\
v_{10}(x, y, 0) &= v_{10}^*(x, y),\\
w_{10}(x, y, 0) &= w_{10}^*(x, y).
\end{aligned} \tag{47}$$

The ground vibration level is often required to be presented in terms of the vibrational velocity rather than the displacement. In this case, differentiating equation (46) with respect to time $t$ gives the vibrational velocities of the ground surface $\dot{u}_{10}(x, y, t)$, $\dot{v}_{10}(x, y, t)$, and $\dot{w}_{10}(x, y, t)$. It can be shown that

$$\dot{u}_{10}(x, y, t) = -c\frac{\partial u_{10}^{*}(x - ct, y)}{\partial (x - ct)} e^{i\Omega t} + i\Omega u_{10}^{*}(x - ct, y) e^{i\Omega t}$$

the Fourier transform of which, denoted by $\bar{\dot{u}}_{10}(x, y, t)$, is

$$\bar{\dot{u}}_{10}(\beta, \gamma, t) = (-c i\beta \tilde{u}_1(\beta, \gamma, 0) + i\Omega \tilde{u}_1(\beta, \gamma, 0)) e^{i(\Omega - \beta c)t} = i(\Omega - \beta c)\tilde{u}_1(\beta, \gamma, 0) e^{i(\Omega - \beta c)t}.$$

Therefore, the Fourier transforms of the vibrational velocities of the ground surface may be calculated as

$$\begin{aligned}
\bar{\dot{u}}_{10}(\beta, \gamma, t) &= i(\Omega - \beta c)\tilde{u}_1(\beta, \gamma, 0) e^{i(\Omega - \beta c)t}, \\
\bar{\dot{v}}_{10}(\beta, \gamma, t) &= i(\Omega - \beta c)\tilde{v}_1(\beta, \gamma, 0) e^{i(\Omega - \beta c)t}, \\
\bar{\dot{w}}_{10}(\beta, \gamma, t) &= i(\Omega - \beta c)\tilde{w}_1(\beta, \gamma, 0) e^{i(\Omega - \beta c)t}.
\end{aligned} \tag{48}$$

## 5. VIBRATIONAL DISPLACEMENT SPECTRA OF THE GROUND SURFACE

Since the load moves, a load of a single frequency in the moving frame of reference will produce a transient response at a fixed point in the ground which has a spectrum containing a range of frequency components, i.e., a Doppler effect takes place based on the speeds of wave propagation in the ground. In order to calculate the spectrum of response of the ground to the moving load of single angular frequency $\Omega$, equation (46) is Fourier transformed with respect to time $t$. Now denoting the frequency domain functions corresponding to

$$u_{10}(x, y, t), v_{10}(x, y, t), w_{10}(x, y, t) \quad \text{by} \quad S_u(x, y, f), S_v(x, y, f), S_w(x, y, f),$$

where $f$ is the frequency on the ground, gives, for example,

$$S_u(x, y, f) = \int_{-\infty}^{\infty} u_{10}(x, y, t) e^{-i2\pi f t} dt = \int_{-\infty}^{\infty} u_{10}^{*}(x - ct, y) e^{-i(2\pi f - \Omega)t} dt.$$

Putting $x - ct = \xi$, then $dt = -1/c\ d\xi$, gives

$$\begin{aligned}
S_u(x, y, f) &= \frac{1}{c}\int_{-\infty}^{\infty} u_{10}^{*}(\xi, y) e^{-i(2\pi f - \Omega)(x - \xi)/c} d\xi \\
&= \frac{1}{c} e^{-i(2\pi f - \Omega)x/c} \int_{-\infty}^{\infty} u_{10}^{*}(\xi, y) e^{i(2\pi f - \Omega)\xi/c} d\xi.
\end{aligned}$$

Now, the quantity $(\Omega - 2\pi f)/c$ defines the wave number in the direction of $c$ (i.e. $\beta$, the wave number in the $x$ direction). This shows that, in calculating the frequency

response at a point on the ground, the frequency ordinate, $f$, can be replaced with an equivalent value of $\beta$ and the calculation performed as

$$\beta = (\Omega - 2\pi f)/c \tag{49}$$

then

$$S_u(x, y, f) = \frac{1}{c} e^{i\beta x} \int_{-\infty}^{\infty} u_{10}^*(\xi, y) e^{-i\beta\xi} d\xi.$$

From equation (45), this becomes

$$S_u(x, y, f) = \frac{1}{c} e^{i\beta x} \left( \frac{1}{2} \int_{-\infty}^{\infty} \tilde{u}_1(\beta, \gamma, 0) e^{i\gamma y} d\gamma \right), \tag{50}$$

where the integration is the inverse Fourier transform of $\tilde{u}_1(\beta, \gamma, 0)$ with respect to $\gamma$. It can be shown in the same way that

$$S_v(x, y, f) = \frac{1}{c} e^{i\beta x} \left( \frac{1}{2} \int_{-\infty}^{\infty} \tilde{v}_1(\beta, \gamma, 0) e^{i\gamma y} d\gamma \right), \tag{51}$$

$$S_w(x, y, f) = \frac{1}{c} e^{i\beta x} \left( \frac{1}{2} \int_{-\infty}^{\infty} \tilde{w}_1(\beta, \gamma, 0) e^{i\gamma y} d\gamma \right) \tag{52}$$

and for the rail and the sleeper, the displacement spectra are

$$S_R(x, f) = \frac{1}{c} e^{i\beta x} \tilde{w}_1(\beta), \tag{53}$$

$$S_S(x, f) = \frac{1}{c} e^{i\beta x} \tilde{w}_2(\beta), \tag{54}$$

where $\beta$ is determined by equation (49), and from equation (16), $\omega = \Omega - \beta c = 2\pi f$.

Equations (50)–(54) show that the amplitudes of the spectra of the ground surface and the rail and sleeper are independent of the value of $x$. This reflects the fact that the spectrum represents the movement through the observation point of the steady state wave field associated with the load moving along the $x$-axis from $x = -\infty$ to $+\infty$.

It is also worth noting that the product of the amplitude of the displacement spectrum and $2\pi f$ gives the amplitude of the velocity spectrum, and that, due to the fact that $Q_{13}(0, \gamma) = 0$ for any $\gamma$ (see section 3), and from equations (44), (49) and (50), $S_u(x, y, f) = 0$ for any $x$ and $y$ when $f = \Omega/2\pi$, i.e., the longitudinal spectrum vanishes at the frequency of the harmonic moving load.

## 6. RESULTS FROM THE MODEL

In this section some results are presented which investigate the generation of the vibration at different load velocities below, near to, and above the wave speed of the

first mode in the ground. For these calculations a simple ground structure has been used. The ground has one layer of soil, 2 m deep which overlies a half-space of stiffer material. A representation of the ground in this way has been shown adequately to represent the behaviour of the real ground sites over the frequency range of interest for the railway-induced vibration [5, 7]. The material properties of the ground vary considerably from one location to another. Here a single set of material parameters has been taken to be the same as the one set used in reference [19]. These parameters represent a realistic, though arbitrary ground. In the following discussion, effects are shown which are a function of the load speed relative to ground wave speeds. For sites with lower wave speeds in the ground, i.e., softer soil, these effects would occur at correspondingly lower load speeds. The material parameters chosen for the layer and the half-space are listed in Table 1. The parameters for the railway track are presented in Table 2.

To aid the interpretation of the results, the dispersion diagram for the ground structure (without track) is shown in Figure 2, i.e., the wave numbers of propagating modes in the ground are plotted against frequency. In this figure, the modes involving coupled compression and vertically polarized shear wave motion (P-SV modes) are marked with solid lines. The modes involving horizontally polarized shear motion (SH modes), which is decoupled from compression, are marked with dotted lines. Since the SH modes have no component of vertical motion and only the vertical track dynamics are modelled, they are not excited in the model.

TABLE 1

*The parameters for the ground*

| layer | depth (m) | Young's modulus ($\times 10^6$ N/m) | The Poisson ratio | Density (kg/m$^3$) | Loss factor | P-wave speed (m/s) | S-wave speed (m/s) | Rayleight wave speed (m/s) |
|---|---|---|---|---|---|---|---|---|
| 1 | 2·0 | 60 | 0·44 | 1500 | 0·1 | 360 | 118 | 112 |
| Half | space | 360 | 0·49 | 2000 | 0·1 | 1750 | 245 | 233 |

TABLE 2

*The parameters for the railway*

| | |
|---|---|
| Mass of rail beam per unit length of track | 120 kg/m |
| Bending stiffness of rail beam | $1{\cdot}26 \times 10^7$ N m$^2$ |
| Rail pad stiffness | $3{\cdot}5 \times 10^8$ N/m$^2$ |
| Rail pad loss factor | 0·15 |
| Mass of sleepers per unit length of track | 490 kg/m |
| Mass of ballast per unit length of track | 1200 kg/m |
| Ballast stiffness per unit length of track | $3{\cdot}15 \times 10^8$ N/m$^2$ |
| Loss factor of ballast | 1.0 |
| Contact width of railway and ground | 2·7 m |

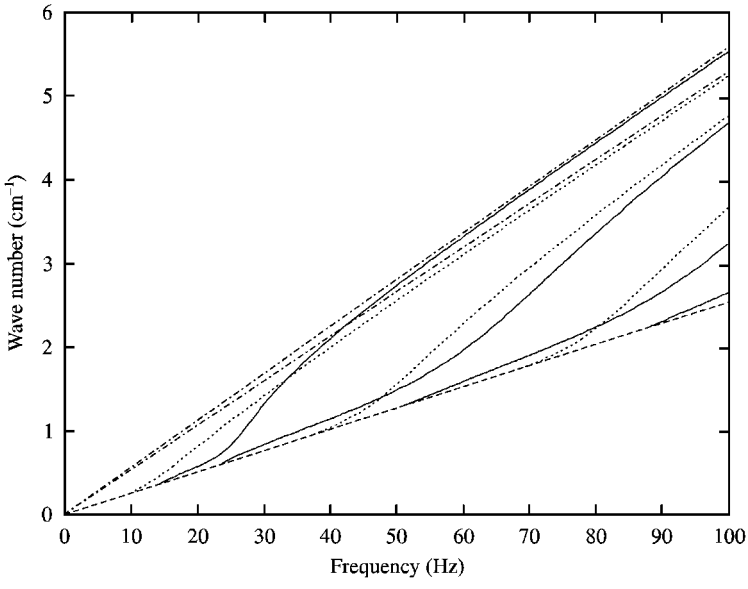


Figure 2. Dispersion diagram for the propagating modes in the ground comprising a single layer over a half-space (no track present) (——— P-SV modes, ····· SH waves, - - - - shear wave of half-space, -·-·- Rayleigh wave and shear wave of a half-space of layer material).

Below about 15 Hz no mode of propagation exists in the layer material. In the frequency range from 15 Hz to approximately 25 Hz a rise in the transmitted vibration occurs due to the onset of propagation in the layer via P-SV modes. The peak in the transfer response occurs at about 25 Hz [19]. Such a rise in the response has been observed in measurements of transfer frequency response functions in the ground and is important in characterizing the spectrum of vibration from trains [5, 7].

At high frequency, the first P-SV mode has a short wavelength compared with the depth of the layer and its wave number converges towards that of a Rayleigh wave in a half-space of the layer material. This is shown in the dispersion diagram (Figure 2) where the Rayleigh wave and shear wave speeds of a half-space of the upper layer material are indicated. It can also be seen that the first SH mode converges towards the wave number of shear waves in the layer material. For the ground parameters chosen, the P-wave speed in the layer is greater than the shear wave speed in the half-space.

From the dispersion diagram it can be seen that at about 24 Hz a second P-SV mode arises and a third appears just above 50 Hz. Figure 3 plots the mode shapes of the two P-SV modes at 40 Hz. The first P-SV mode is tied to deformation of the layer material while the second mode has a higher component of deformation of the substratum material.

### 6.1. NON-HARMONIC MOVING LOAD RESULTS

Figure 4 shows the response of the surface of the ground for the model with the track and a constant vertical unit load moving at 83 m/s. The response is plotted as

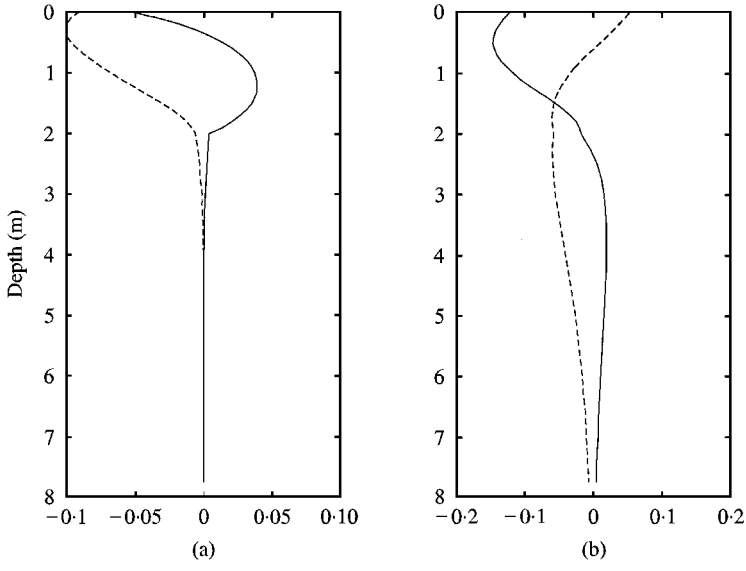


Figure 3. The two P-SV mode shapes at 40 Hz (undamped solution), (a) wave number = 2·1/m, (b) wave number = 1·145/m (——— lateral and, - - - - vertical displacements plotted at $\pi/4$ phase from $t = 0$).

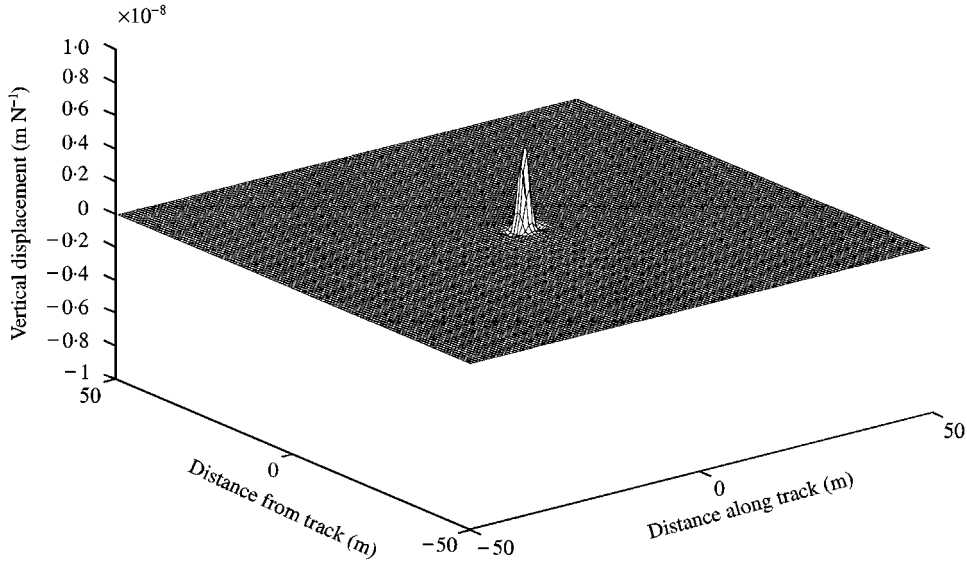


Figure 4. The vertical response of the layered ground surface for a constant load on the track moving at 83 m/s.

a function of distance from the track ($y$) and the distance from the load along the track in the moving frame of reference ($x - ct$). The direction of movement is to the right of the figure. In this representation the vertical axis shows downward displacement as positive. For this and subsequent similar plots, the phase

information is retained by showing the displacement at an instant in time. For this speed, which is below the wave speeds in the ground, the displacement forms a simple dip in the surface of the ground localized under the load. The effect of the bending stiffness of the track can be seen as an upward displacement ahead of and behind the load. The deformation pattern is said to be quasi-static, i.e., although it is not quite symmetric in $(x - ct)$, it still resembles the deformation pattern under a static load on the track.

Figure 5 shows the deformation for a speed of 112 m/s, i.e., at the Rayleigh wave speed of the upper layer material. In this case, a greater amplitude of displacement occurs at the loading point and a displacement is observable at greater distances along the track than for the lower speed of load. A small "bow wave" can be seen at the load position which extends a little distance to the side of the track. For comparison with Figure 5, Figure 6 shows the "bow wave" for the load moving at the same speed for the track resting on a half-space of the layer material. In this case the increase in amplitude is much greater and the effect of the bow wave extends a long way to the side of the track. This demonstrates that the layered structure of the ground is important in determining the occurrence and the amplitude of the effects associated with the loads moving at critical velocities of the ground.

The effects of a further increase of speed to 150 m/s, for the layer on half-space ground, are shown in Figure 7. At this speed, in excess of the Rayleigh wave speed of the layer material, a number of waves are created in the track behind the load. These create propagating waves in a "Mach cone" behind the moving load. Waves are also generated in the track ahead of the load because of the bending stiffness of the rails. This phenomenon can also be seen in an analysis of a moving load on a beam with an elastic foundation (see for example reference [20]). The peak deflection of the track for the 150 m/s load is greater than that at 112 m/s and it has

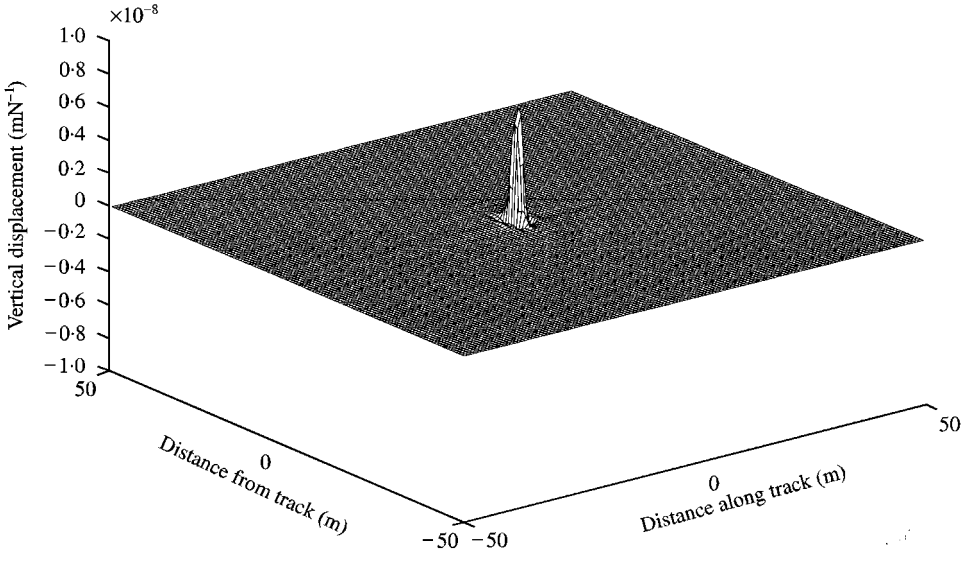


Figure 5. The vertical response of the layered ground surface for a constant load on the track moving at 112 m/s.

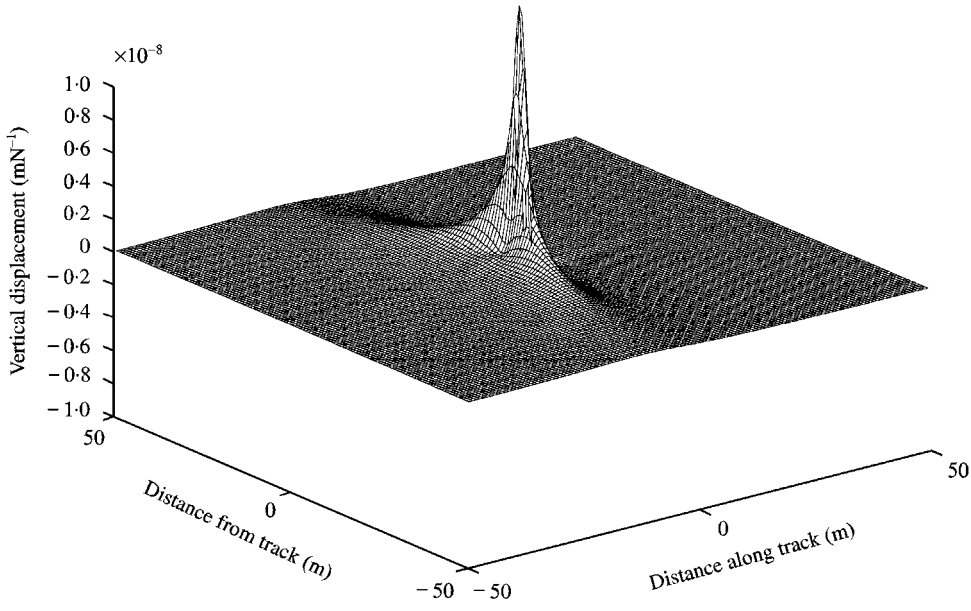


Figure 6. The vertical response of the ground surface for a constant load on the track moving at 112 m/s where the ground is modelled only as a half-space of the layer material.

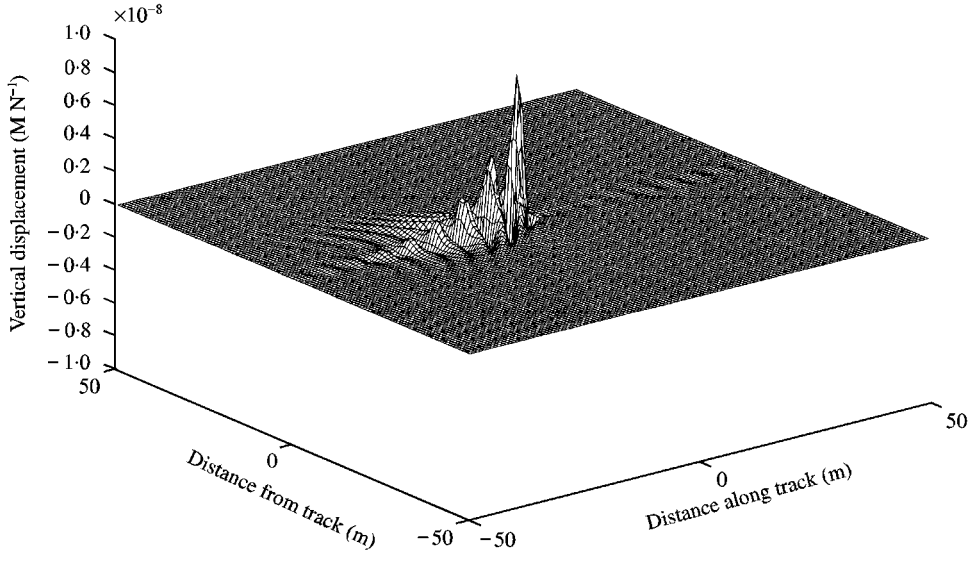


Figure 7. The vertical response of the surface of the layered ground for a constant load on the track moving at 150 m/s.

been found that the deflection of the track under the loading point goes through a maximum at around this load speed.

For a fixed-point load of finite frequency, the propagating modes of the ground that are excited by the load are simply the modes existing at that frequency as

indicated by the dispersion diagram (Figure 2). For a moving load, modes are excited via the velocity of the load according to the Doppler effect. From equation (16) it can be seen that the line $\beta = |(\Omega - 2\pi f)|/c$, where $c$ is the load speed, indicates that the wave numbers excited (here the modulus is used to make the line indicate the excitation of both the directions of the wave propagation in the ground with respect to the direction of the movement of the load whilst still only plotting the positive wave numbers). For a constant load $\Omega = 0$. Figure 8 therefore shows the P-SV modes of Figure 2 overlaid with the lines $\beta = 2\pi f/c$ for $c = 83$, 112, 150, 180 and 230 m/s. Figure 8 therefore indicates the modal wave numbers that are excited.

At the load speed of 150 m/s, the load speed line intersects the first P-SV mode at about 25 Hz at which the response function of the layered ground is at its maximum. Therefore the amplitude of response of the ground goes through a maximum at this load speed.

When the load travels at a speed near to the Rayleigh wave speed of the half-space substratum (230 m/s), Figure 9, two angles of Mach cone can be seen, one for the waves in the layer, the other for the waves more closely associated with the half-space. The latter propagate to greater distances than the waves in the layer.

Figure 10 shows the spectrum of vertical displacement at $y = 0$ m (i.e., under the track) for the load passing by. For speeds greater than the Rayleigh wave speed of the layer material, a rise occurs in the spectrum between 15 and 25 Hz corresponding to the onset of modal propagation in the layer. A peak is observed at a frequency close to which the load-speed line intersects the dispersion curve for the first P-SV mode (Figure 8). (Recall that the dispersion diagram does not take into account the modification of the first P-SV mode wave number by the presence of the track.) The peak occurs at a slightly lower frequency for the higher load speeds

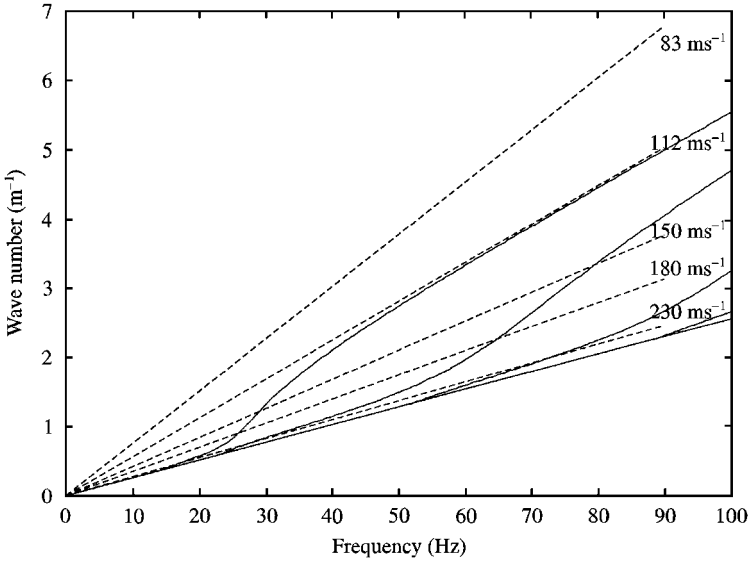


Figure 8. Dispersion diagram for the P-SV modes of the layered ground (no track present) with load speed lines overlaid for a constant load.

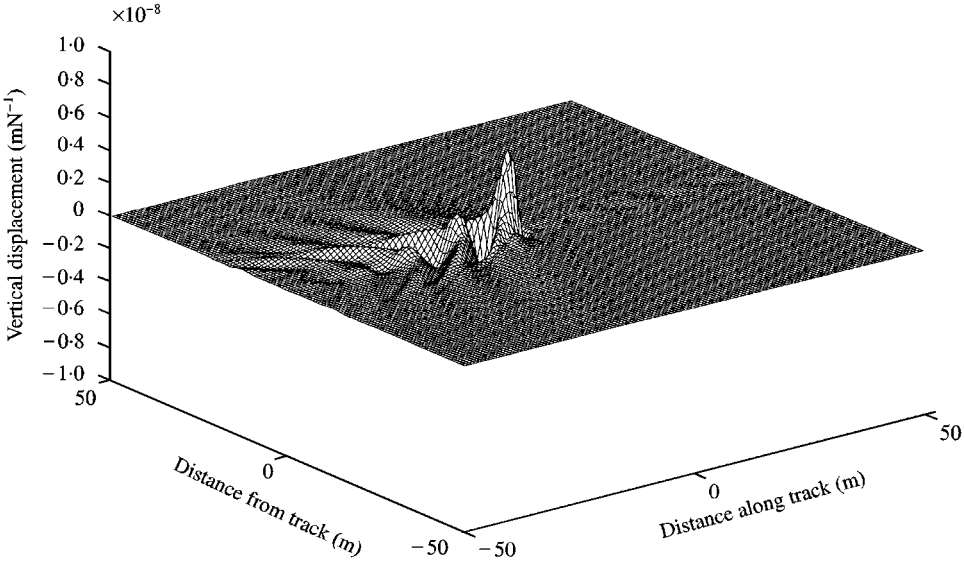


Figure 9. The vertical response of the surface of the layered ground for a constant load on the track moving at 230 m/s.

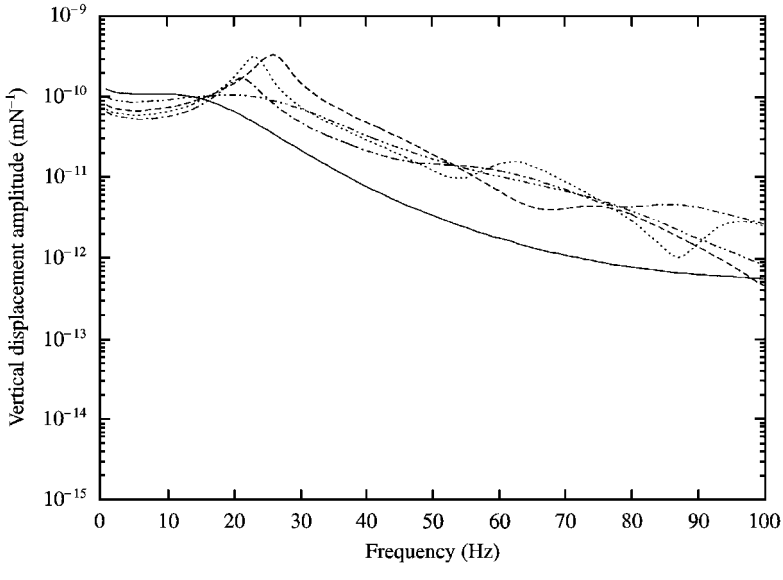


Figure 10. Spectrum of vertical displacement at a fixed point under the track ($y = 0$ m) during the pass-by of a unit constant vertical load at various load speeds (——— 83 m/s, ·-·-·-· 112 m/s, - - - - 150 m/s, ····· 180 m/s, -·-·- 230 m/s).

than for the lower wave speeds. Peaks at higher frequencies corresponding to the intersections with higher order modes can also be seen. These peaks are broad because of the level of damping in the ground. For the 83 m/s load speed, the spectrum shape is smooth representing the passage of the quasi-static deflection

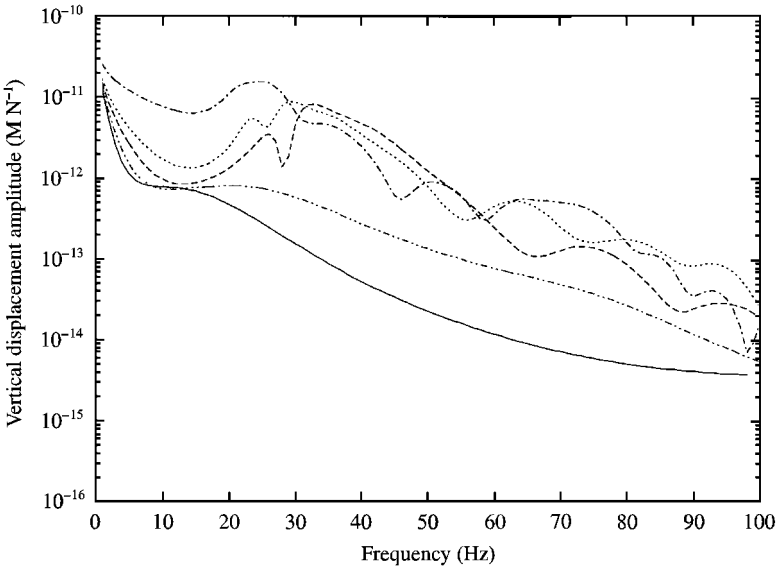


Figure 11. Spectrum of vertical displacement at a fixed point 10 m from the track centre-line during the pass-by of a unit constant vertical load at various speeds (——— 83 m/s, ·-·-·- 112 m/s, - - - - 150 m/s, ····· 180 m/s, -·-·- 230 m/s).

curve through the observation point and no excitation of the modes occurs. For this reason the level of the response to this speed of load is lower than for the higher load speeds. The fact that the highest level of response is at 150 m/s can be seen in this figure.

Figure 11 shows the spectrum of vertical displacement for a fixed point of the ground surface at $y = 10$ m from the track centreline. Comparison with Figure 10 shows a greater attenuation over the 10 m distance from the track for the 83 m/s load speed than for the higher speeds that excite propagating modes. The effects of summation of contributions of vibration from points along the track give the spectra for the higher load speed cases a more complicated frequency content than for the point under the track.

### 6.2. RESULTS FOR A HARMONIC MOVING LOAD

Attention is now given to some results for a non-zero frequency load. For this purpose a frequency of 40 Hz at which two P-SV modes exist, has been chosen. The mode shapes have already been presented in Figure 3. Results for a number of frequencies, covering some variations in the ground properties and track structure have been presented in a previous paper [19]. For this reason a limited set of results is presented in this section.

Figure 12 shows the response of the ground to a unit amplitude load of 40 Hz frequency, moving at 83 m/s. By plotting the results for an instant in time at which the sinusoidal load is at its maximum, rather than as amplitude, the propagating

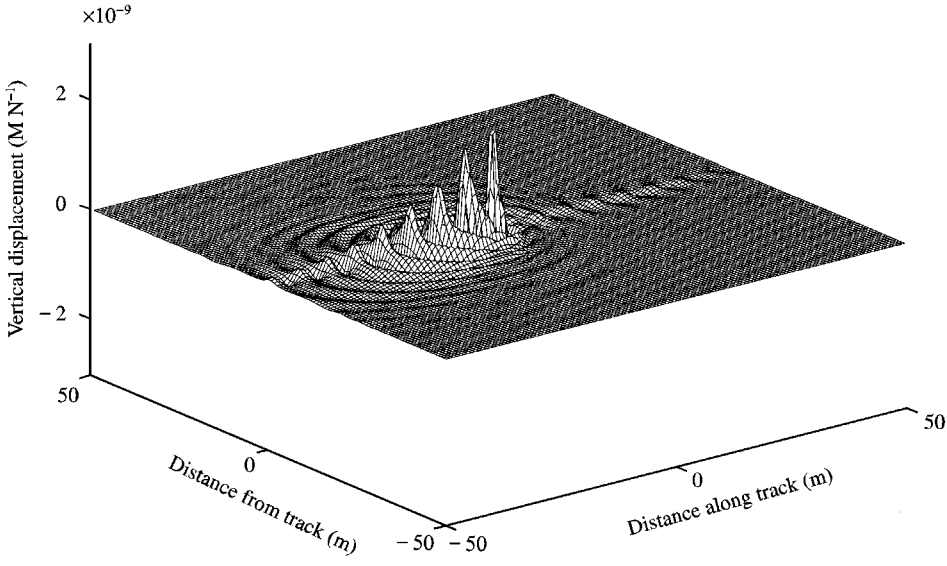


Figure 12. Vertical response of the ground surface to a 40 Hz load moving along the track at 83 m/s in the moving frame of reference.

waves can be seen. At this speed, the effect of the movement of the load is evident in the asymmetry of wave propagation and in the fact that the waves under the track trail more behind the load than in the front. Waves in the ground propagate with concentric wave fronts.

The situation at 150 m s, being faster than the Rayleigh wave speed in the upper layer, is shown in Figure 13. The 40 Hz frequency can be seen to result in a longer wavelength along the track (in $x - ct$) because of the higher load speed. In this case also, waves can be seen propagating ahead of the load under the track because of the bending stiffness of the rails (cf. Figure 7 for the constant moving load). In this case however, the wave fronts that can be seen, which are due to the two propagating modes, are confined to a Mach cone behind the load. Two different angles of this can be discerned relating to the two modes of propagation. Despite the fact that Figure 12 is for a train speed below the Rayleigh wave speed and that Figure 13 is for a train speed above it, the displacement amplitude of waves at this frequency, shown in Figures 12 and 13 are of similar order of magnitude. (This is also true for load speeds of 40 and 112 m/s which are presented in reference [19].)

The spectrum of response at a fixed point 10 m from the track due to the pass-by of a single frequency load of 40 Hz at a speed of 83 m/s is presented in Figure 14. Unlike the presentation of results hitherto, this figure shows the amplitude of all the three components of displacement. Amplitudes of the vertical, lateral and longitudinal components of the response are of the same order of magnitude.

The fact that a single-frequency load moving along the track produces a transient with a broad band spectrum at a fixed point in the ground is a manifestation of the Doppler effect. In the simple case of a single propagating wave speed, the effect of a moving source is to produce a pass-by spectrum with frequency content bounded

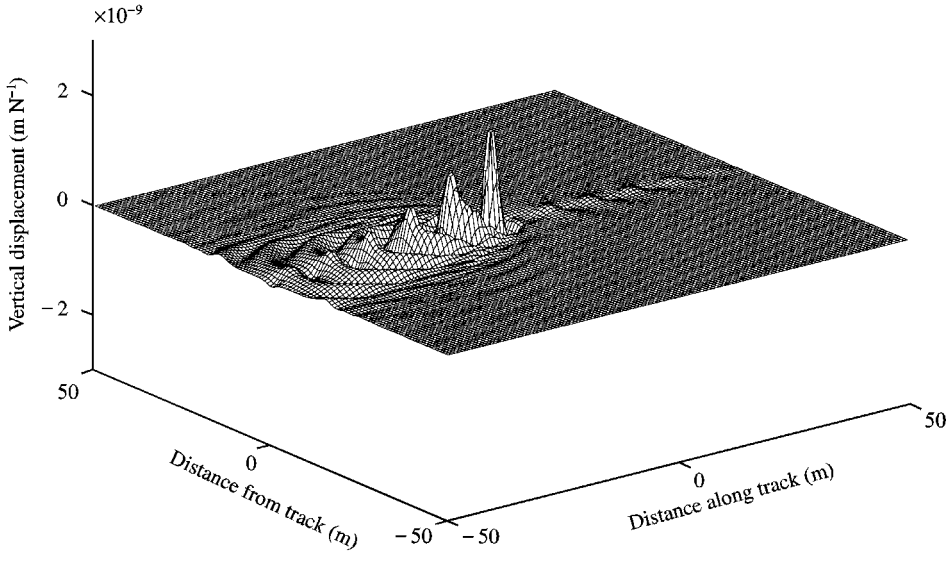


Figure 13. Vertical response of the ground surface to a 40 Hz load moving along the track at 150 m/s in the moving frame of reference.

by two peaks corresponding to the frequencies, $f$, defined by $f = f_s\ c_0/(c_0 \pm u_s)$ where $c_0$ is the velocity of propagation in the medium and $u_s, f_s$ are the speed of the movement and frequency of the source. In the case of the propagation in damped, layered ground, a continuous function of wave speed exists with peaks at the modal wave speeds. As already seen, the modal wave speeds correspond to the intersections of the dispersion curves for the P-SV modes with the line defined by $\beta = |(\Omega - 2\pi f)|/c$. Figure 15 shows load speed lines for 40 Hz loads moving at 83, 112 and 150 m/s plotted on the dispersion diagram. For the load speed of 83 m/s, energy carried by the first P-SV mode would form broad peaks around 26 and 150 Hz, and for the second P-SV mode at approximately 29 and 62 Hz. Higher wave speeds, pertaining to the propagation via wave speeds of the half-space, result in the energy being spread over smaller band-widths about the 40 Hz load frequency, i.e., between these frequencies. The frequencies indicated above can be seen to be reflected in the shape of the spectrum of Figure 14. The effect at the lower bound of observed frequency for the two P-SV modes (26 and 29 Hz) is to form a sharp cut-off in the spectrum below these frequencies in Figure 14.

For load speeds at, or above, the wave speeds in the ground, the range of frequencies excited in the ground becomes infinite. Figure 16 shows the spectrum at the ground point for a load speed of 150 m/s. It can be seen that the peak in response occurs at a slightly lower frequency of about 24 Hz in this case and a greater response level occurs at high frequencies.

Comparison of the curve for 83 m/s in Figure 11 with Figure 14 shows that at frequencies above 20 Hz, the response to the 40 Hz load exceeds the response to the constant load. By 30 Hz the response to the 40 Hz load is the greater by a factor of about 100. Below 20 Hz the response at 10 m from the constant load exceeds that

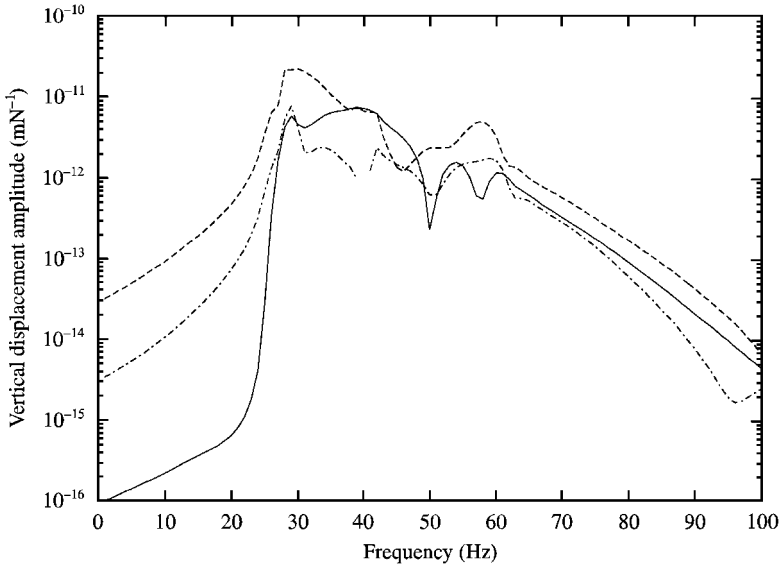


Figure 14. Spectrum of the vertical (———), lateral (– – –) and longitudinal (-·-·-) displacement observed at a fixed positon in the ground 10 m from the centreline of the track for a 40 Hz load moving along the track at 83 m/s.

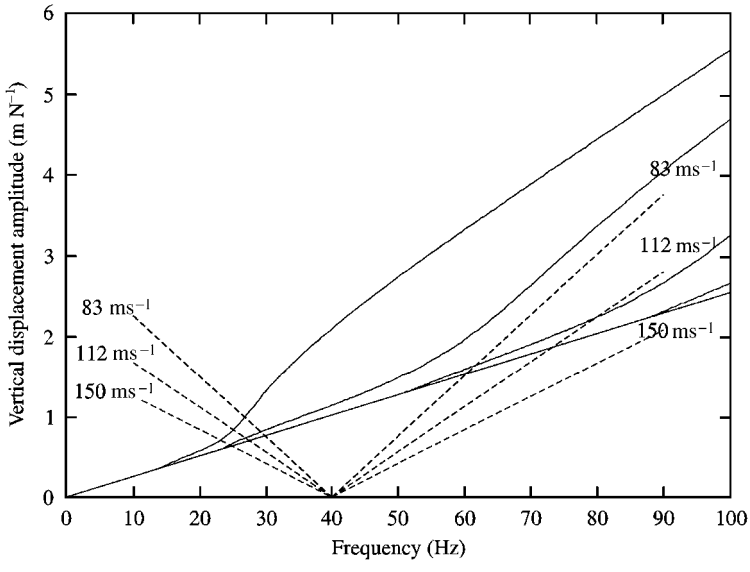


Figure 15. Dispersion diagram for the P-SV modes of the layered ground with load speed lines overlaid for a 40 Hz load.

from the 40 Hz load. Considering the load speed of 150 m/s, although the response to the constant load is much greater than for the 83 m/s load (Figure 11) for frequencies above 20 Hz, it is still only of the same order of magnitude as the response to the 40 Hz dynamic load at its peak around 30 Hz.

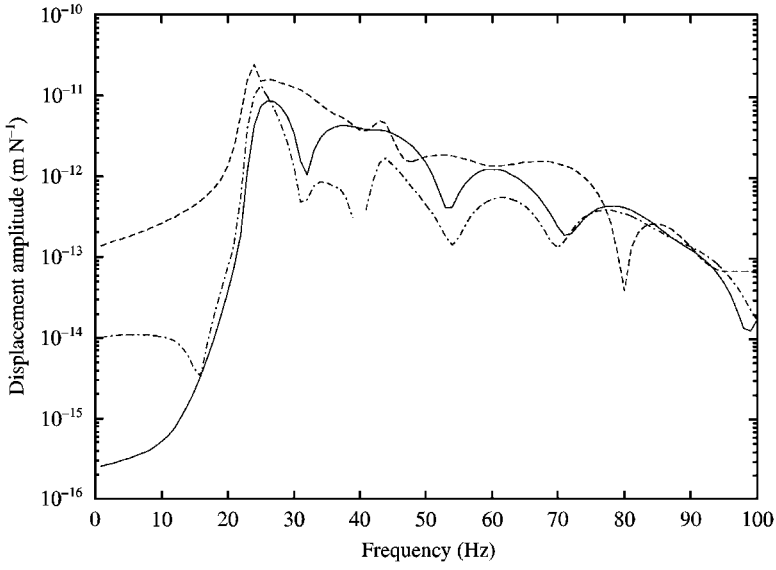


Figure 16. Spectra of the vertical (———), lateral (– – –) and longitudinal (-·-·-) displacement observed at a fixed positon in the ground 10 m from the centreline of the track for a 40 Hz load moving along the track at 150 m/s.

The relative magnitudes of the constant load compared to the dynamic load applied by the wheels of a railway vehicle moving at high speed is not evaluated in the present work. However, reference [21] provides an example of the contact force measured on the wheel although the speed is only 20 m/s. In those measurements, a high-pass filter has been applied to eliminate the strong components of force due to the modes of the vehicle on its suspension for frequencies below 10 Hz. From the results presented, dynamic forces in the range of about 20–40 Hz can be seen to have an amplitude of a few per cent of the static load value. This is increased considerably in measurements on a wheel when a wheel flat is introduced. Although the cases of reference [21] and the cases on which the comparison of Figures 11 and 14 are made are not compatible, the general conclusion may be drawn that both the static and the dynamic forces applied by the vehicle are likely to contribute significantly, in different frequency bands, to the vibration measured at points away from the track.

## 7. CONCLUSIONS

A method of calculating the vibration response of a layered ground subject to a harmonic load moving along the rails of a railway track has been proposed. The model may be used to analyse three components of vibration generated by the wheels of a train, namely (a) dynamic loads generated at a fixed point on the track, (b) the moving constant axle loads, and (c) moving dynamic loads applied through the wheels.

Calculations from the model have been used to show some characteristics of moving-load induced vibration of a layered ground structure consisting of a single

layer overlying a half-space of stiffer material. These have been interpreted in the light of the dispersion curve for propagating modes in the ground.

A constant load moving at a speed below any of the wave speeds in the ground produces only a quasi-static response pattern in the ground surface away from the track. At load speeds higher than the Rayleigh wave speed of the upper layer material, propagating waves are produced. In the layered ground structure no great increase in the amplitude of the ground response is observed for a load moving at the Rayleigh wave speed as is the case when the ground is modelled as a half-space of this material. For higher load speeds, higher amplitudes occur at particular speeds and waves of high amplitude propagating to large distances occur near to the Rayleigh wave speed of the half-space substratum in the model. Calculations of the spectrum of response to a moving constant load at the track and 10 m away show a significant increase in the response to loads travelling faster than the Rayleigh wave speed in the layer above the frequency related to the onset of the propagating modes in the layer. In this case, since propagating modes are excited (as they are by the dynamic load), the rate of decay of vibration with distance away from the track is lower than that for the quasi-static response for constant loads at speeds below the ground wave speeds.

The model has been used to calculate the displacement spectrum at a point away from the track due to a single-frequency component of dynamic load moving on the track. These show that vertical, lateral and longitudinal components of the response are of comparable order of magnitude at this distance and that, for high-speed loads, a single-frequency component in the load gives rise to a broad-band response in the ground. The magnitudes of the responses to the zero frequency moving load and the dynamic loads at a point away from the track indicate that both quasi-static and dynamic loads are likely to be significant in the spectrum of the train vibration in different frequency bands. Even in the case of trains travelling at speeds in excess of the ground wave speeds, the dynamic loads are likely to be significant compared to the "bow wave" from the quasi-static loads for frequencies above the onset of the modal propagation in the layer.

## ACKNOWLEDGMENT

C. J. C. Jones wishes to acknowledge the financial support for his participation in this work of the EPSRC under research grant GR/L11397.

## REFERENCES

1. P. Nelson 1987 *Transportation Noise Reference Book*. London: Butterworths.
2. V. V. Krylov 1995 *Applied Acoustics* **44**, 149–164. Generation of ground vibration by superfast trains.
3. C. Madshus and A. Kaynia 1998 *Proceedings of the Sixth International Workshop on Railway Noise, Île des Embiez, France*, 108–119. High speed railway lines on soft ground: dynamic behaviour at critical train speed.
4. V. V. Krylov 1998 *Ground Dynamics and Man Made Processes* (B. O. Skipp, T. Telford, editors) 69–86. Effect of layered ground on ground vibrations generated by high speed trains.

5. C. J. C. Jones 1994 *Proceedings of the Institution of Civil Engineers, Transportation* **105**, 43–51. Use of numerical models to determine the effectiveness of anti-vibration systems for railways.
6. X. Sheng, C. J. C. Jones and M. Petyt 1999 *Journal of Sound and Vibration* **225**(1), 3–28. Ground vibration generated by a harmonic load acting on a railway track.
7. C. J. C. Jones and J. R. Block 1996 *Journal of Sound and Vibration* **193**, 205–213. Prediction of ground vibration from freight trains.
8. H. Takemiya and K. Goda 1998 *Structural Engineering/Earthquake Engineering, JSCE* 605/I-45, 161–169. Wave propagation /impediment in a soil stratum over rigid base due to impulse/moving loads. (in Japanese).
9. B. Alabi 1989 *Applied Mathematical Modelling* **13**, 710–715. A model for the problem of ground vibration induced by the wheels of a moving train.
10. B. Alabi 1992 *Journal of Sound and Vibration* **153**, 77–87. A parameter study on some aspects of groundborne vibration due to rail traffic.
11. D. V. Jones, D. Le Houedec, A. T. Peplow and M. Petyt 1998 *European Journal of Mechanics A/Solids* **17**, 153–166. Ground vibration in the vicinity of a moving harmonic rectangular load on a half space.
12. F. C. P. De Barros and J. E. Luco 1994 *Wave Motion* **19**, 189–210. Response of a layered viscoelastic half-space to a moving point load.
13. N. Haskell 1953 *Bulletin of the Seismological Society of America* **73**, 17–43. The dispersion of surface waves on multilayered media.
14. W. T. Thomson 1950 *Journal of Applied Physics* **21**, 81–93 Transmission of elastic waves through a stratified soil medium.
15. H. A. Dieterman and A. Metrikine 1997 *Journal of Applied Mechanics, Transaction of the ASME* **64**, 596–600. Critical velocities of a harmonic load moving uniformly along an elastic layer.
16. H. A. Dieterman and A. Metrikine 1997 *European Journal of Mechanics A/Solids*, **16**, 295–306. Steady-state displacements of a beam on an elastic half-space due to a uniformly moving constant load.
17. E. Kausel and J.M. Roësset 1981 *Bulletin of the Seismological Society of America* **71**, 1743–1761. Stiffness matrices for layered soils.
18. X. sheng, C.J.C. jones and M. Petyt 1999 *University of Southampton, Institute of Sound and Vibration Research, Technical Memorandum* 837. The Fourier transformed stationary and moving dynamic flexibility matrices of a layered ground.
19. C. J. C. Jones, X. sheng and M. Petyt 1999 *Journal of Sound and Vibration*. Simulations of ground vibration from a moving harmonic load on a railway track (accepted).
20. L. Frýba 1972 *Vibration of Solids and Structures Under Moving Loads*. Groningen: Noordhoff International Publishing.
21. M. Fermér and J. C. O. Nielsen 1995 *Proceedings of the Institution of Mechanical Engineers* **209**, 39–47. Vertical interaction between train and track with soft and stiff railpads—full scale experiments and theory.